Analysis of Separation in Turbulent Incompressible Flow

Johan Hoffman and Claes Johnson

July 12, 2011

Abstract

We present a scenario of stable 3d rotational separation in high Reynolds number slightly viscous incompressible turbulent flow around a solid body such as an airplane, car or boat, supported by computation, mathematical analysis and experimental observation. Our scenario is fundamentally different from the scenario of unstable 2d irrotational separation in viscous flow advocated by Prandtl in 1904 signifying the birth of modern fluid mechanics of viscous flow as a development of classical fluid mechanics of inviscid potential flow presented by Euler and d'Alembert. Our scenario allows a description of high Reynolds number slightly viscous flow past a solid body as inviscid potential flow before separation followed by 3d rotational separation. We show that the pressure distribution of 3d rotational separation is a determining factor for both drag and lift.

1 From Unstable to Stable Separation

In this note we present an analysis of the fundamental problem of fluid mechanics of the motion of a solid body, such as a subsonic airplane, car or boat, through a slightly viscous incompressible fluid such as air at subsonic speeds or water. We focus on incompressible flow at large Reynolds number (of size 10^6 or larger) around both bluff and streamlined bodies, which is always partly turbulent.

The basic problem is to determine the forces acting on the surface of the body from the motion through the fluid, with the *drag* being the total force in the direction of the flow and the *lift* the total force in a transversal direction to the flow.

As a body moves through a fluid initially at rest, like a car or airplane moving through still air, or equivalently as a fluid flows around a body at rest, approaching fluid particles are deviated by the body in contracting flow, switch to expanding flow at a crest and eventually leave the body. The flow is said to *attach* in the front and *separate* in the back as fluid particles approach and leave a proximity of the body surface.

In high Reynolds number slightly viscous flow the tangential forces on the surface, or *skin friction* forces are small and both drag and lift mainly result from pressure forces and the pressure distribution at turbulent separation is of particular concern.

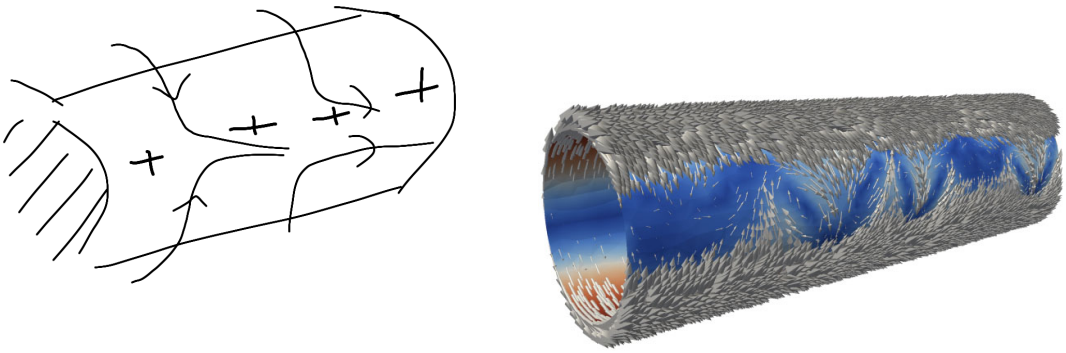

Figure 1: Irrotational separation of potential flow around a circular cylinder (left) from line of stagnation surrounded by a high pressure zone indicated by $+$, with corresponding opposing surface flow instability (right) .

Separation requires *stagnation* of the flow to zero velocity somewhere in the back of the body as opposing flows are meeting. Stagnation requires *retardation* of the flow, which requires a streamwise increasing pressure, or *adverse pressure gradient*. We show by a linearized stability analysis that retardation from opposing flows is exponentially unstable, which in particular shows potential flow to be unstable. Since unstable flow cannot persist over time, we expect to find a *quasi-stable* separation pattern resulting from the most unstable mode of potential flow, as a flow without streamwise retardation from opposing flows. By quasi-stable we mean a flow which is not exponentially unstable and thus may have a certain permanence over time.

Both experiment and computation show that there is such a quasi-stable separation pattern arising from transversal reorganization of opposing potential flow

in the back into a set of counter-rotating vortex tubes of swirling flow (streamwise vorticity) attaching to the body, accompanied by a zig-zag pattern of alternating low and high pressure zones around points of stagnation with low pressure inside the vortex tubes. This pattern is illustrated in Fig. 1 for a cylinder along with computation and experiment, where we see how the flow finds a way to separate with unstable streamwise retardation in opposing flows replaced by quasi-stable transversal accelleration close to the surface before separation and in the swirling flow after separation. We see this phenomenon in the swirling flow in a bathtub drain, which is a stable configuration with transversal accelleration replacing the unstable opposing flow retardation of fully radial flow.

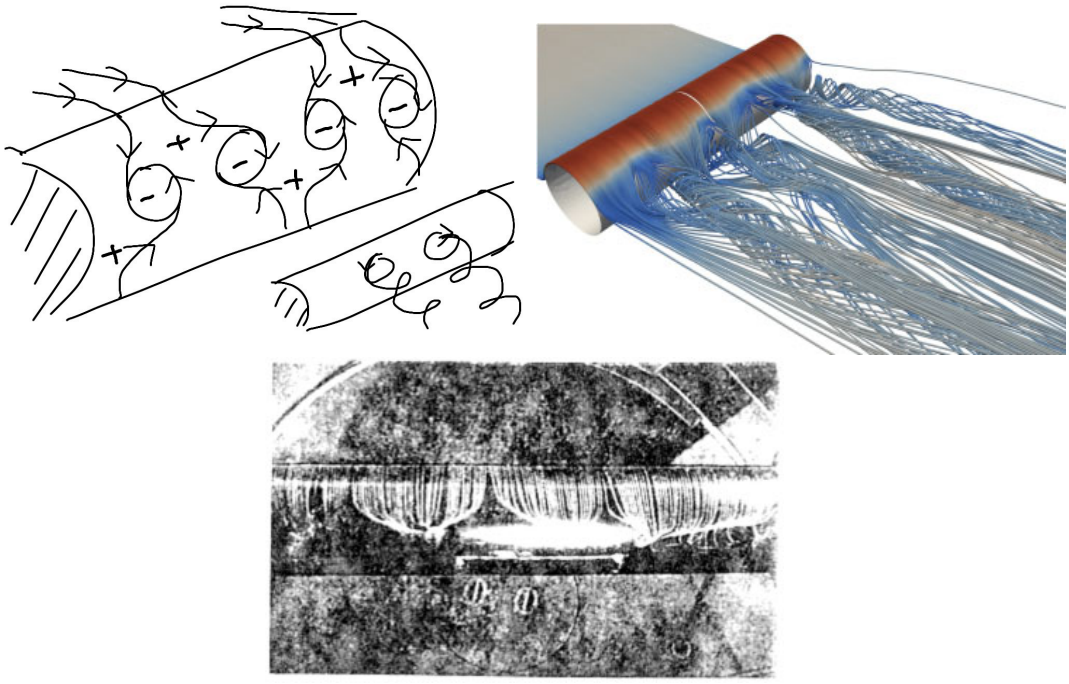

Figure 2: 3d rotational separation from alternating high/low pressure: principle, computation and experiment

We refer to this quasi-stable pattern as *3d rotational separation*. This is a macroscopic phenomenon with the stagnation points spaced as widely as possibe. From macroscopic point of view the small skin friction of slightly viscous flow can be modeled with a *slip boundary condition* expressing vanishing skin fric-

tion. We show that computational solution of Navier-Stokes equations with slip is possible at affordable cost, because with slip there are no boundary layers to resolve, which makes it possible to compute both drag and lift of a of a car, boat or airplane arbitrary shape without the quadrillions of mesh points for boundary layer resolution commonly believed to be required [20].

The single high pressure zone stretching along the stagnation line of potential flow around a circular cylinder (creating instability) as shown in Fig. 1, is thus broken down into a pattern of high and low pressure zones by the development of low pressure vortical flow, which allows the fluid to separate without unstable streamwise retardation in opposing flow. The so modified pressure creates drag of a bluff body and lift of a wing from the zero drag and lift of potential flow.

2 Resolution of D'Alembert's Paradox

A potential solution can be viewed as an approximate solution of the Navier-Stokes equations at high Reynolds number with a slip boundary condition, but a potential solution is unphysical because both drag and lift are zero, as expressed in d'Alembert's paradox [15]. Inspection of potential flow shows unstable *irrotational separation* of retarding opposing flow, which is impossible to observe as a physical flow. D'Alembert's paradox is thus resolved by observing that potential flow with zero drag and lift is unstable [15] and thus unphysical, and not by the official resolution suggested by Prandtl stating that the unphysical feature is the slip boundary condition.

Although 3d rotational separation has a macroscopic features the flow is *turbulent* at separation in the sense that the dissipation in the flow is substantial even though the viscosity is very small, following the definition of turbulent flow in [14].

3 Main Result

We present evidence in the form of mathematical stability analysis, computation and observation, that high Reynolds number incompressible flow around a body moving through a fluid can be described as

- quasi-stable potential flow before separation,
- quasi-stable 3d rotational separation.

We show that both drag and lift critically depend on the pressure distribution of 3d rotational separation. We remark that in the attaching flow in the front the flow is retarded by the body and not by opposing flows as in the back, which allows stable potential flow attachment. We show that drag and lift of a body of arbitrary shape can be accurately computed by solving the Navier-Stokes equations with slip.

The description and analysis of the crucial flow feature of separation presented here is fundamentally different from that of Prandtl, named the father of modern fluid mechanics, based on the idea that both drag and lift originate from a thin viscous boundary layer, where the flow speed relative to the body rapidly changes from the free stream speed to zero at the body surface corresponding to a no-slip boundary condition. Prandtl's scenario for separation, which has dominated 20th century fluid, can be described as *2d boundary layer no-slip separation*, to be compared with our entirely different scenario of *3d no-boundary layer slip separation*.

The unphysical aspect of Prandtl's scenario of separation is illuminated in [18]:

- *The passage from the familiar 2d to the mysterious 3d requires a complete reconsideration of concepts apparently obvious (separation and reattachment points, separated bubble, recirculation zone) but inappropriate and even dangerous to use in 3d flows*.

4 The Incompressible Navier-Stokes Equations with Slip

We study separation in high Reynolds number slightly viscous incompressible flow through the *Navier-Stokes equations* for an *incompressible* fluid of unit density with *small viscosity* $\nu > 0$ and *small skin friction* $\beta \geq 0$ filling a volume Ω in $\mathbb{R}^3$ surrounding a solid body with boundary Γ over a time interval $I = [0, T]$: Find the velocity $u = (u_1, u_2, u_3)$ and pressure p depending on $(x, t) \in \Omega \cup \Gamma \times I$, such that

$$\begin{aligned} \dot{u} + (u \cdot \nabla)u + \nabla p - \nabla \cdot \sigma &= f && \text{in } \Omega \times I, \\ \nabla \cdot u &= 0 && \text{in } \Omega \times I, \\ u_n &= g && \text{on } \Gamma \times I, \\ \sigma_s &= \beta u_s && \text{on } \Gamma \times I, \\ u(\cdot, 0) &= u^0 && \text{in } \Omega, \end{aligned} \tag{1}$$

where $\dot{u} = \frac{\partial u}{\partial t}$, u_n is the fluid velocity normal to Γ, u_s is the tangential velocity, $\sigma = 2\nu\epsilon(u)$ is the stress with $\epsilon(u)$ the usual velocity strain, σ_s is the tangential stress, f is a given volume force, g is a given inflow/outflow velocity with $g = 0$ on a non-penetrable boundary, and u^0 is a given initial condition. We notice the skin friction boundary condition coupling the tangential stress σ_s to the tangential velocity u_s with $\beta = \frac{U}{2}c_f$, where $c_f = \frac{2\tau}{U^2}$ is the *skin friction coefficient*, with $\beta = 0$ for slip (and $\beta >> 1$ for no-slip).

Experiments show that the skin friction coefficient decreases with increasing Reynolds number Re as $c_f \approx 0.05 \sim Re^{-0.2}$, so that $c_f \approx 0.0005$ for $Re = 10^{10}$ and $c_f \approx 0.005$ for $Re = 10^5$. Accordingly we model a turbulent boundary layer by friction boundary condition with a friction parameter $\beta \approx 0.03URe^{-0.2}$ and in the case of very large Reynolds number wih $\beta = 0$ corresponding to slip.

We show in [14, 12, 15] that the Navier-Stokes equations (1) can be solved by a stabilized finite element referred to as *G2* as an acronym for General Galerkin. G2 produces turbulent solutions characterized by substantial turbulent dissipation from the least squares stabilization acting as an automatic turbulence model, reflecting that the Navier-Stokes residual cannot be made small in turbulent regions. G2 has a posteriori error control based on duality and shows output uniqueness in mean-values such as lift and drag [14, 11, 10, 13]

We find that G2 with slip is capable of modeling slightly viscous turbulent flow with $Re > 10^6$ of relevance in many applications in aero/hydro dynamics, including flying, sailing, boating and car racing, with hundred thousands of mesh points in simple geometry and millions in complex geometry, while according to state-of-the-art quadrillions is required [20]. This is because a friction-force/slip boundary condition can model a turbulent boundary layer, and interior turbulence does not have to be resolved to physical scales to capture mean-value outputs [14].

5 Stability Analysis by Linearization

The stability of a Navier-Stokes solution is expressed by the linearized equations

$$\begin{array}{rcll} \dot{v} + (u\cdot\nabla)v + (v\cdot\nabla)\bar{u} + \nabla q &=& f - \bar{f} & \text{in } \Omega\times I,\\ \nabla\cdot v &=& 0 & \text{in } \Omega\times I,\\ v\cdot n &=& g-\bar{g} & \text{on } \Gamma\times I,\\ v(\cdot,0) &=& u^0-\bar{u}^0 & \text{in } \Omega, \end{array} \tag{2}$$

where (u,p) and $(\bar{u},\bar{p})$ are two Euler solutions with slightly different data, and $(v,q) \equiv (u-\bar{u}, p-\bar{p})$. Formally, with u and $\bar{u}$ given, this is a linear convection-

reaction problem for (v, q) with growth properties governed by the reaction term given by the 3×3 matrix $\nabla \bar{u}$. By the incompressiblity, the trace of $\nabla \bar{u}$ is zero, which shows that in general $\nabla \bar{u}$ has eigenvalues with real values of both signs, of the size of $|\nabla u|$ (with $|\cdot|$ some matrix norm), thus with at least one exponentially unstable eigenvalue, except in the neutrally stable case with purely imaginary eigenvalues, or in the non-normal case of degenerate eigenvalues representing parallel shear flow [14].

The linearized equations in velocity-pressure indicate that, as an effect of the reaction term $(v \cdot \nabla)\bar{u}$:

- streamwise retardation is exponentially unstable in velocity,
- transversal accelleration is neutrally stable,

where transversal signifies a direction orthogonal to the flow direction.

Additional stability information is obtained by applying the curl operator $\nabla\times$ to the momentum equation to give the vorticity equation

$$\dot{\omega} + (u \cdot \nabla)\omega - (\omega \cdot \nabla)u = \nabla \times f \quad \text{in } \Omega, \tag{3}$$

which is also a convection-reaction equation in the vorticity $\omega = \nabla \times u$ with coefficients depending on u, of the same form as the linearized equation (5), with a sign change of the reaction term. The vorticity is thus locally subject to exponential growth with exponent $|\nabla u|$:

- streamwise accelleration is exponentially unstable in streamwise vorticity.

We sum up as follows: The linearized equations (5) and (5) indicate exponential growth of perturbation of velocity in streamwise retardation and of streamwise vorticity in streamwise accelleration. We shall see in more detail below 3d rotational separation results from exponential instability of potential flow in retardation followed by vortex stretching in accelleration, with the retardation replaced by neutrally stable transversal accelleration.

Note that in classical analysis it is often argued that from the vorticity equation (5), it follows that vorticity cannot be generated starting from potential flow with zero vorticity and $f = 0$, which is *Kelvin's theorem*. But this is an incorrect conclusion, since perturbations of $\bar{f}$ of f with $\nabla \times \bar{f} \neq 0$ must be taken into account, even if $f = 0$. What you effectively see in computations is local exponential growth of vorticity on the body surface in rear retardation and by vortex stretching in accelleration, even if $f = 0$, which is a main route of instability to turbulence as well as separation.

6 Exponential Instability of 2d Irrotational Separation

We now analyze the stability of 2d irrotational separation considered by Planck in the following model of the potential flow around a circular cylinder studied in more detail below: $u(x) = (x_1, -x_2, 0)$ in the half-plane $\{x_1 > 0\}$ with stagnation along the line $(0, 0, x_3)$ and

$$\frac{\partial u_1}{\partial x_1} = 1 \quad \text{and} \quad \frac{\partial u_2}{\partial x_2} = -1, \tag{4}$$

expressing that the fluid is *squeezed* by *retardation* in the x_2-direction and *accelleration* in the x_1-direction. We first focus on the retardation with the main stability feature of (5) captured in the following simplified version of the v_2-equation of (5), assuming x_1 and x_2 are small,

$$\dot{v}_2 - v_2 = f_2,$$

where we assume $f_2 = f_2(x_3)$ to be an oscillating perturbation depending on x_3 of a certain wave length δ and amplitude h, for example $f_2(x_3) = h\sin(2\pi x_3/\delta)$, expecting the amplitude to decrease with the wave length. We find, assuming $v_2(0, x) = 0$, that

$$v_2(t, x_3) = (\exp(t) - 1)f_2(x_3).$$

We next turn to the accelleration and then focus on the ω_1-vorticity equation, for x_2 small and $x_1 \geq \bar{x}_1 > 0$ with $\bar{x}_1$ small, approximated by

$$\dot{\omega}_1 + x_1\frac{\partial \omega_1}{\partial x_1} - \omega_1 = 0,$$

with the "inflow boundary condition"

$$\omega_1(\bar{x}_1, x_2, x_3) = \frac{\partial v_2}{\partial x_3} = (\exp(t) - 1)\frac{\partial f_2}{\partial x_3}.$$

The equation for ω_1 thus exhibits exponential growth, which is combined with exponential growth of the "inflow condition". We can see these features in principle and computational simulation in Fig. 1 showing how opposing flows at separation generate a pattern of alternating surface vortices from pushes of fluid up/down, which act as initial conditions for vorticity stretching into the fluid generating counter-rotating low-pressure tubes of streamwise vorticity.

The above model study can be extended to the full linearized equations linearized at $u(x) = (x_1, -x_2, 0)$:

$$\begin{aligned} Dv_1 + v_1 &= -\frac{\partial q}{\partial x_1}, \\ Dv_2 - v_2 &= -\frac{\partial q}{\partial x_2} + f_2(x_3), \\ Dv_3 &= -\frac{\partial q}{\partial x_3}, \\ \nabla \cdot v &= 0 \end{aligned} \tag{5}$$

where $Dv = \dot{v} + u \cdot \nabla v$ is the convective derivative with velocity u and $f_2(x_3)$ as before. We here need to show that the force perturbation $f_2(x_3)$ will not get cancelled by the pressure term $-\frac{\partial q}{\partial x_2}$ in which case the exponential growth of v_2 would get cancelled. Now $f_2(x_3)$ will induce a variation of v_2 in the x_3 direction, but this variation does not upset the incompressibility since it involves the variation in x_2. Thus, there is no reason for the pressure q to compensate for the force perturbation f_2 and thus exponential growth of v_2 is secured.

We thus find streamwise vorticity generated by a force perturbation oscillating in the x_3 direction, which in the retardation of the flow in the x_2-direction creates exponentially increasing vorticity in the x_1-direction, which acts as inflow to the ω_1-vorticity equation with exponential growth by vortex stretching. Thus, we find exponential growth at rear separation in both the retardation in the x_2-direction and the accelleration in the x_1 direction, as a result of the squeezing expressed by (4).

Since the combined exponential growth is independent of δ, it follows that large-scale perturbations with large amplitude have largest growth, which is also seen in computations with δ the distance between streamwise rolls as seen in Fig. 5 which does not seem to decrease with decreasing h. The perturbed flow with swirling separation is large scale phenomenon, which we show below is more stable than potential flow.

The corresponding pressure perturbation changes the high pressure at separation of potential flow into a zig-zag alternating more stable pattern of high and low pressure with high pressure zones deviating opposing flow into non-opposing streaks which are captured by low pressure to form rolls of streamwise vorticity allowing the flow to spiral away from the body. This is similar to the vortex formed in a bathtub rain.

Notice that in attachment in the front the retardation does not come from opposing flows but from the solid body, and the zone of exponential growth of ω_2 is short, resulting in much smaller perturbation growth than at rear separation.

We shall see that the tubes of low-pressure streamwise vorticity change the normal pressure gradient to allow separation without unstable retardation, but the

price is generation of drag by negative pressure inside the vortex tubes as a "cost of separation".

7 Quasi-Stable Rotational 3d Separation

We discover in computation and experiment that the rotational 3d separtion pattern just detected as the most unstable mode of 2d, represents a quasi-stable flow with unstable retardation in opposing flows replaced by transversal acceleration.

As a model of flow with transversal accelleration we consider the potential velocity $u = (0, x_3, -x_2)$ of a constant rotation in the x_1-direction, with corresponding linearized equations linearized problem

$$\dot{v}_1 = 0, \quad \dot{v}_2 + v_3 = 0, \quad \dot{v}_3 - v_2 = 0, \tag{6}$$

which model a neutrally stable harmonic oscillator without exponential growth corresponding to imaginary eigenvalues of ∇u.

Further, shear flow may represented by $(x_2, 0, 0)$, which is marginal unstable with linear perturbation growth from degenerate zero eigenvalues of ∇u, as analyzed in detail in [14].

8 Quasi-Stable Potential Flow Attachment

The above analysis also shows that potential flow attachment, even though it involves streamwise retardation, is quasi-stable. This is because the initial perturbation f_2 in the above analysis is forced to be zero by the slip boundary condition requiring the normal velocity to vanish. In short, potential flow attachment is stable because the flow is retarded by the solid body and not by opposing flows as in separation.

This argument further shows that a flow retarded by a high pressure zone is quasi-stable in approach because it is similar to attachment.

9 Circular Cylinder

We consider the flow around a around a long circular cylinder of unit radius with axis along the x_3-axis in $\mathbb{R}^3$ with coordinates $x = (x_1, x_2, x_3)$, assuming the flow velocity is $(1, 0, 0)$ at infinity.

9.1 Unstable Unphysical Potential Flow

Potential flow as inviscid, irrotational, incompressible stationary flow, is given in polar coordinates (r, θ) in a plane orthogonal to the cylinder axis by the potential function, see Fig. 3,

$$\varphi(r,\theta) = (r + \frac{1}{r})\cos(\theta)$$

with corresponding velocity components

$$u_r \equiv \frac{\partial \varphi}{\partial r} = (1 - \frac{1}{r^2})\cos(\theta), \quad u_s \equiv \frac{1}{r}\frac{\partial \varphi}{\partial \theta} = -(1 + \frac{1}{r^2})\sin(\theta)$$

with streamlines being level lines of the conjugate potential function

$$\psi \equiv (r - \frac{1}{r})\sin(\theta).$$

Potential flow is constant in the direction of the cylinder axis with velocity $(u_r, u_s) =$

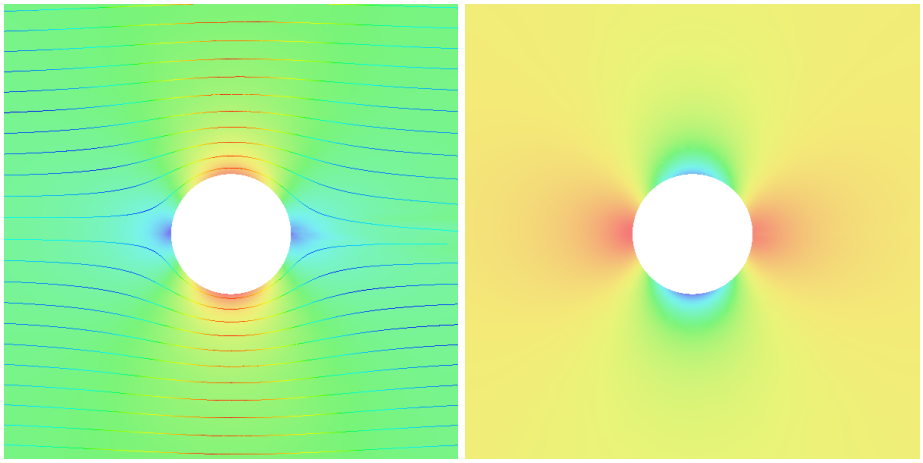

Figure 3: Potential flow past a circular cylinder: fully symmetric velocity (left) and pressure (right).

$(1, 0)$ for r large, is fully symmetric with zero drag/lift, attaches and separates at the lines of stagnation $(r, \theta) = (1, \pi)$ in the front and $(r, \theta) = (1, 0)$ in the back. Potential flow shows exponentially unstable 2d irrotational separation but quasi-stable 2d attachment. Potential flow thus represents physical flow before separation but not in separation and after separation.

By Bernouilli's principle the pressure is given by

$$p = -\frac{1}{2r^4} + \frac{1}{r^2}\cos(2\theta)$$

when normalized to vanish at infinity. We compute

$$\frac{\partial p}{\partial \theta} = -\frac{2}{r^2}\sin(2\theta)), \quad \frac{\partial p}{\partial r} = \frac{2}{r^3}(\frac{1}{r^2} - \cos(2\theta)),$$

and discover an adverse pressure gradient in the back. Further, the normal pressure gradient on the boundary

$$\frac{\partial p}{\partial r} = 4\sin^2(\theta) \geq 0$$

is precisely the force required to accelerate fluid particles with speed $2|\sin(\theta)|$ to follow the circular boundary without separation, by satisfying the condition of non-separation on a curve with curvature R

$$\frac{\partial p}{\partial n} = \frac{U^2}{R}. \tag{7}$$

We note, coupling to the above discussion relating to (**??**), that $\frac{\partial u_s}{\partial r} = \frac{2}{r^3}\sin(\theta) = 2$ at the crest. We further compute

$$\frac{\partial \psi}{\partial r} = \frac{1}{r^2}\sin(\theta)$$

which shows that fluid particles decrease their distance to the boundary in front of the cylinder and increase their distance in the rear, but the flow only separates at rear stagnation.

9.2 Quasi-Stable Physical Turbulent Flow

Solving Navier-Stokes equations with very small viscsoity and slip boundary condition by G2 we find the a a flow initialized as potential flow develops into a turbulent solution with rotational separation as identified above, in shown in Fig. 4 and 5.

10 NACA0012 Trailing Edge Separation

The separation at the trailing edge of a wing is similar to that of a circular cylinder, as shown in Fig. 10 for a NACA012 wing at 5 degrees angle of attack.

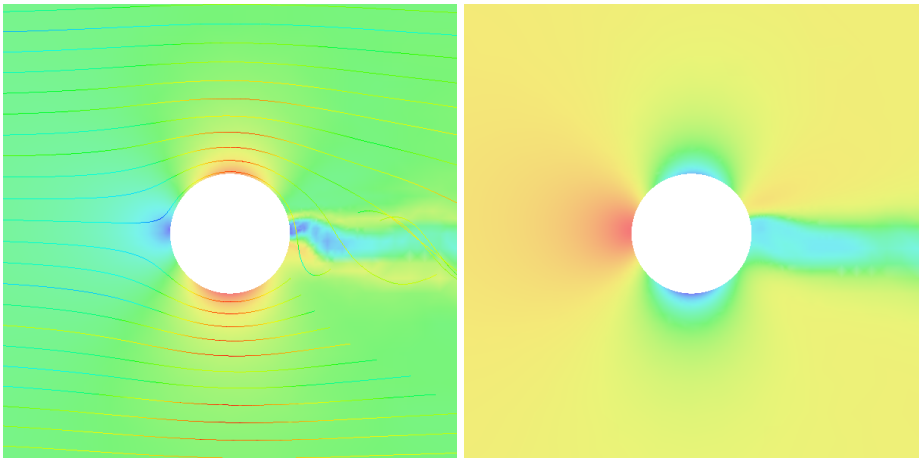

Figure 4: Turbulent flow past a cylinder; velocity (left) and pressure (right). Notice the low pressure wake of strong streamwise vorticity generating drag.

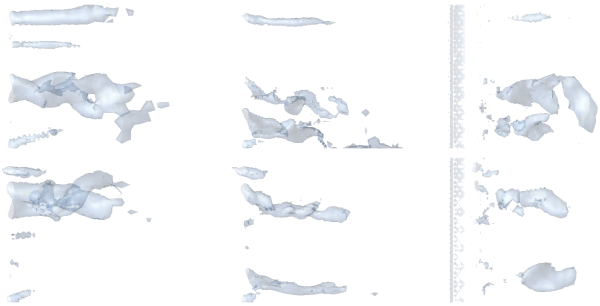

Figure 5: Levels surfaces of strong vorticity in EG2 solution: streamwise $|\omega_1|$ (left) and transversal $|\omega_2|$ (middle) and $|\omega_3|$ (right), at two times $t_1 < t_2$ (upper, lower), in the x_1x_3-plane.

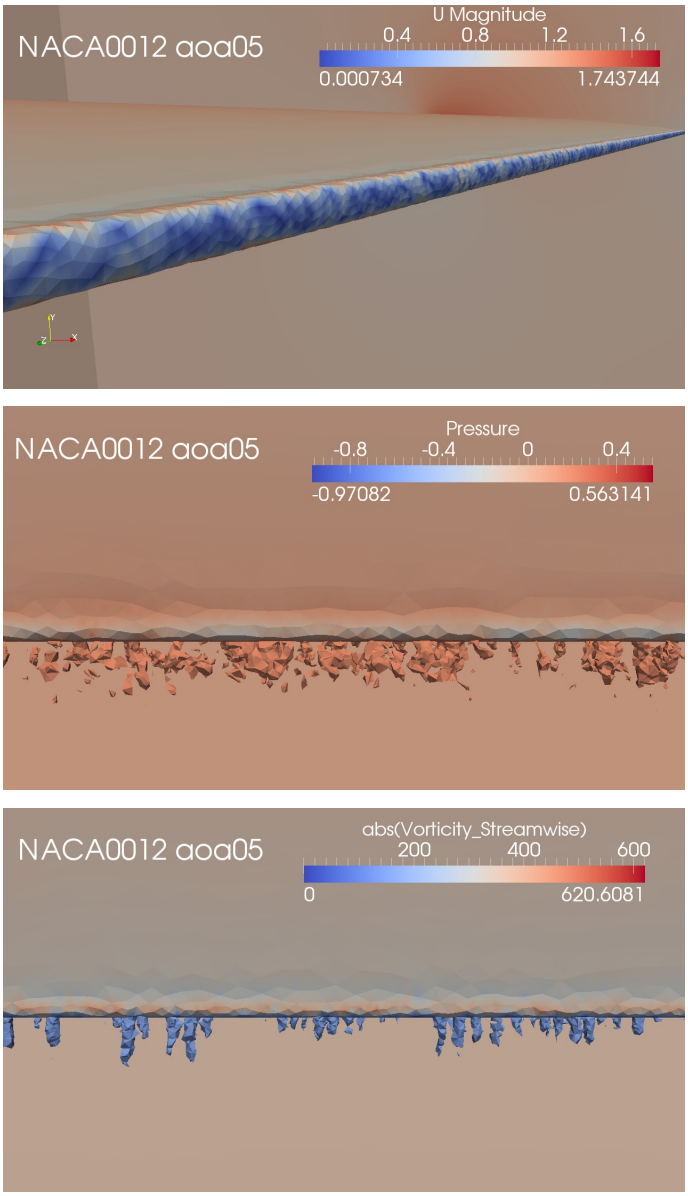

Figure 6: Velocity, pressure and vorticity at trailing edge separation for NACA0012 wing. Notice the zig-zag pattern of the velocity.

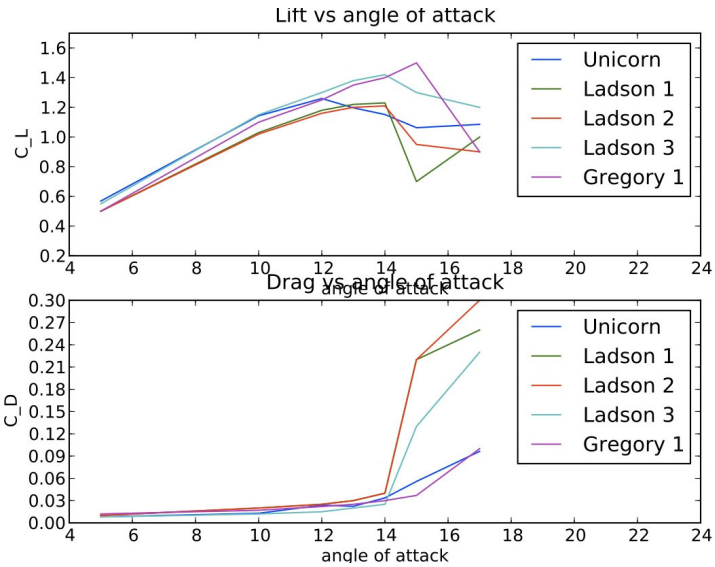

Figure 7: Evidence that drag and lift of a wing can be computed by solving the Navier-Stokes equations with slip without resolving any boundary layers.

11 Accuracte Drag and Lift without Boundary Layer

We compare in Fig. 14 drag and lift of a long NACA0012 wing for different angles of attack including stall computed by solving the of Navier-Stokes equations with slip using Unicorn **??**, with different experiments and notice good agreement. We conclude that drag and lift are computable without resolving and boundary layers.

12 Sphere

Potential flow around a sphere is exponentially unstable at its point of stagnation at separation and develops a quasi-stable separation pattern of four counterrotating rolls of streamwise vorticity as shown in Fig. **??**.

13 Hill

In Fig. 9 we show turbulent Euler flow over a hill with separation after the crest by again the mechanism of tangential separation through generation of surface

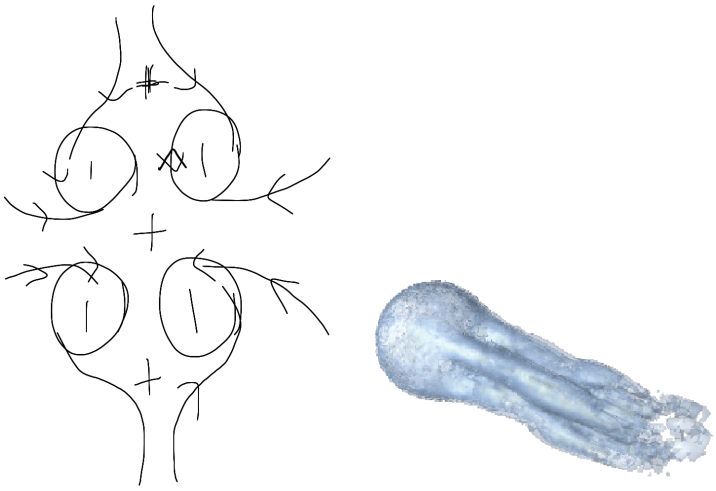

Figure 8: Pattern of exponential instability of potential flow at the point of stagnation of potential flow around a sphere forming four counterrotating rolls of streamwise vorticity shown in computation.

vorticity.

14 Flat Plate

The experience reported above suggests the following scenario for separation into a turbulent boundary layer over a flat plate as a representation of a smooth boundary: (i) Rolls of streamwise vorticity are formed by non-modal linear perturbation growth referred to as the *Taylor Görtler mechanism* in [14]. (ii) The rolls create opposing transversal flows (as in the back of cylinder), which generate surface vorticity which is stretched into the fluid while being bent into to streamwise direction, as evidenced in e.g. [6, 7].

References

[1] John D. Anderson, Ludwig Prandtl's Boundary Layer, http://www.aps.org/units/dfd/resources/upload/prandtlvol58no12p4248.pdf

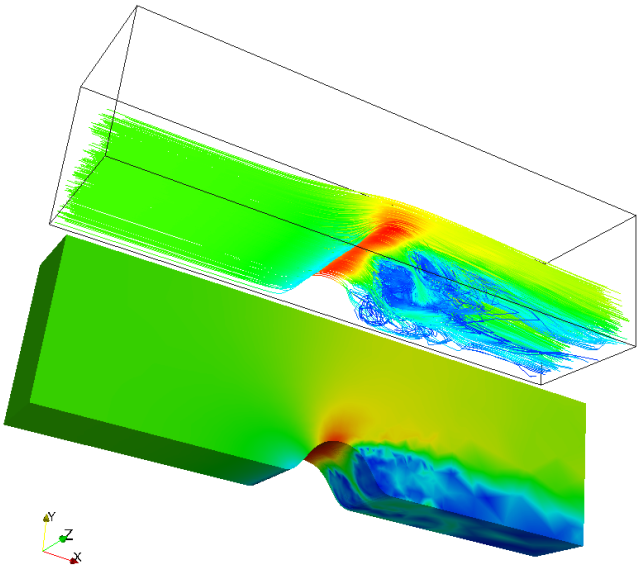

Figure 9: Separation after crest of hill by surface vorticity from opposing flow.

[2] Y. Bazilevs, C. Michler, V.M. Calo and T.J.R. Hughes, Turbulence without Tears: Residual-Based VMS, Weak Boundary Conditions, and Isogeometric Analysis of Wall-Bounded Flows, Preprint 2008.

[3] G. Birkhoff, Hydrodynamics, Princeton University Press, 1950.

[4] S. Cowley, Laminar boundary layer theory: A 20th century paradox, Proceedings of ICTAM 2000, eds. H. Aref and J.W. Phillips, 389-411, Kluwer (2001).

[5] A. Crook, Skin friction estimation at high Reynolds numbers and Reynolds-number effects for transport aircraft, Center for Turbulence Research, 2002.

[6] A. Ferrante, S. Elghobashi, P. Adams, M. Valenciano, D. Longmire, Evolution of Quasi-Streamwise Vortex Tubes and Wall Streaks in a Bubble-Laden Turbulent Boundary Layer over a Flat Plate, Physics of Fluids 16 (no.9), 2004.

[7] A. Ferrante and S. E. Elghobashi, A robust method for generating inflow conditions for direct numerical simulations of spatially-developing turbulent boundary layers, J. Comp. Phys., 198, 372-387, 2004.

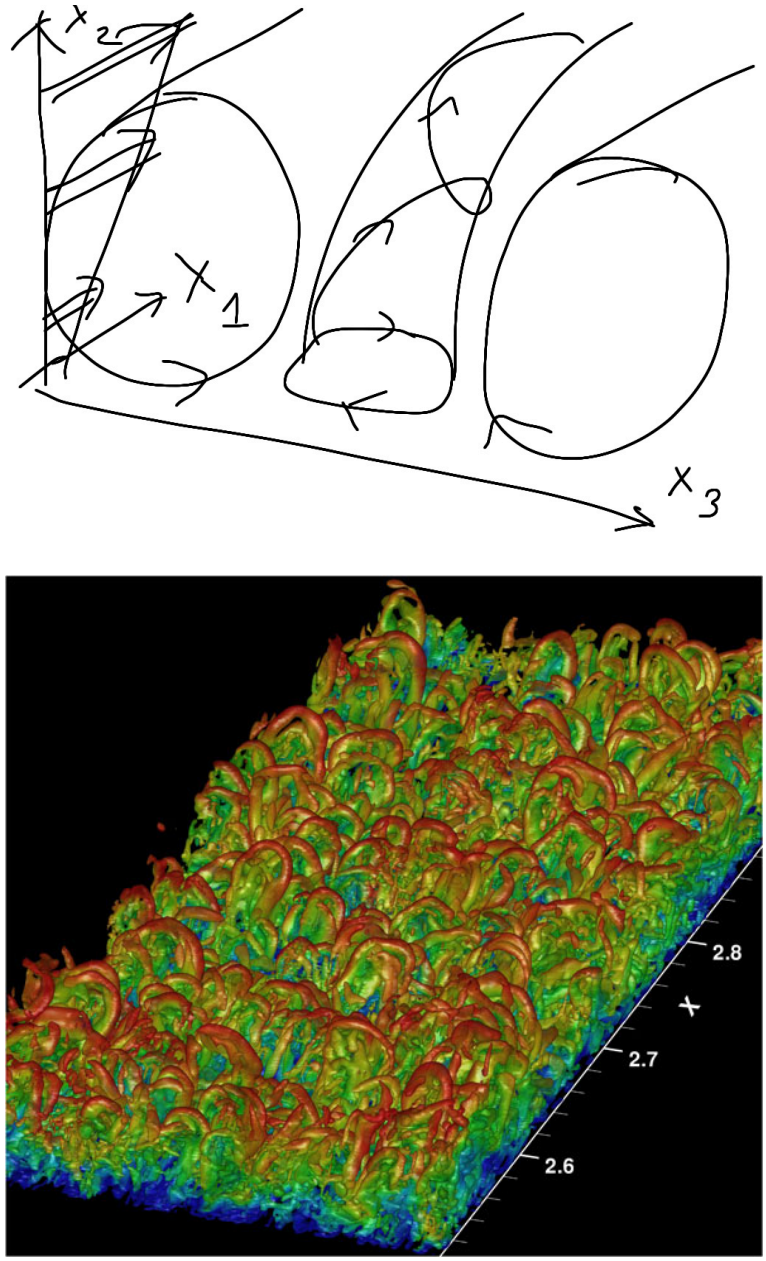

Figure 10: Shear flow over flat plate generates x_1 vorticity which generates secondary transversal opposing flow which generates rolls of x_2-vorticity attaching to the plate and bending into the flow, like a forest of sea tulips attaching to the sea bottom.

[8] J.Hoffman, Simulation of turbulent flow past bluff bodies on coarse meshes using General Galerkin methods: drag crisis and turbulent Euler solutions, Comp. Mech. 38 pp.390-402, 2006.

[9] J. Hoffman, Simulating Drag Crisis for a Sphere using Friction Boundary Conditions, Proc. ECCOMAS, 2006.

[10] J. Hoffman, Lift and drag of a delta wing by EG2.

[11] J. Hoffman, Drag and lift of a car by EG2.

[12] J. Hoffman and C. Johnson, Blowup of Euler solutions, BIT Numerical Mathematics, Vol 48, No 2, 285-307.

[13] J. Hoffman and C. Johnson, Mathematical Theory of Flight, 2009.

[14] J. Hoffman and C. Johnson, Computational Turbulent Incompressible Flow, Springer 2007, home page at www.bodysoulmath.org/books.

[15] J. Hoffman and C. Johnson, Resolution of d'Alembert's paradox, Journal of Mathematical Fluid Mechanics, Online First Dec 10, 2008.

[16] J. Hoffman and C. Johnson, Modeling Turbulent Boundary Layers by Small Friction.

[17] J. Hoffman and Claes Johnson, Knol articles.

[18] J. M. Delery, R. Legendre and Henri Werle: Toward the elucidation of three-dimensional separation, Annu. Rev. Fluid. Mech. 2001 33:129-54.

[19] K. Stewartson, D'Alembert's Paradox, SIAM Review, Vol. 23, No. 3, 308-343. Jul., 1981.

[20] J. Kim and P. Moin, Tackling Turbulence with Supercomputer, Scientific American.

[21] F. W. Lancaster, *Aerodynamics*, 1907.

[22] Article in Ny Teknik.

[23] L. Prandtl, On Motion of Fluids with Very Little Viscosity, Third International Congress of Mathematics, Heidelberg, 1904.

[24] H. Schlichting, Boundary Layer Theory, McGraw-Hill, 1979.

[25] James J. Stoker, Bul.l Amer. Math Soc.

[26] D. You and P. Moin, Large eddy simulation of separation over an airfoil with synthetic jet control, Center for Turbulence Research, 2006.